Distributed Array of GPS Receivers for 3D Wind Profile Determination in Wind Farms

Derek Chen, Liang Heng, Dan Jia, and Grace Xingxin Gao
University of Illinois at Urbana-Champaign

BIOGRAPHY

Derek Chen is currently a senior in the Department of Aerospace Engineering at the University of Illinois at Urbana-Champaign. He is expecting to graduate in May 2014 with a Bachelor of Science and is looking to pursue further graduate studies. His research interests are in autonomous systems, remote sensing and signal processing.

Liang Heng is a postdoctoral research associate in the Department of Aerospace Engineering, University of Illinois at Urbana-Champaign. He received the B.S. and M.S. degrees from Tsinghua University, China in 2006 and 2008, and the Ph.D. degree from Stanford University in 2012, all in Electrical Engineering. His research interests are in cooperative navigation and satellite navigation. He is a member of the Institute of Electrical and Electronics Engineer (IEEE) and the Institute of Navigation (ION).

Dan Jia is an undergraduate in the Department of Aerospace Engineering, University of Illinois at Urbana-Champaign. He is minoring in Physics. His research interests are fluid mechanics, aerodynamics, and aircraft stability and control. He is a James Scholar in Engineering Department, and has been on the Dean's List for four consecutive semesters.

Grace Xingxin Gao is an assistant professor in the Aerospace Engineering Department at University of Illinois at Urbana-Champaign. She received her B.S. degree in Mechanical Engineering in 2001 and her M.S. degree in Electrical Engineering in 2003, both at Tsinghua University, China. She obtained her Ph.D. degree in Electrical Engineering at Stanford University in 2008. Before joining Illinois at Urbana-Champaign as an assistant professor in 2012, Prof. Gao was a research associate at Stanford University. Prof. Gao has won a number of awards, including RTCA William E. Jackson Award, Institute of Navigation Early Achievement Award, 50 GNSS Leaders to Watch by GPS World Magazine, and multiple best presentation awards at ION GNSS conferences.

ABSTRACT

Wind energy is currently one of the fastest growing sources of renewable energy. Sensing the wind profile densely, accurately, in three dimensional, and inexpensively is critical for both optimizing the installation of wind turbines on a wind farm, and predicting and optimizing the power generation. This paper presents a new method of wind profile sensing based on a distributed array of GPS receivers. In our wind sensing system, GPS receivers, wireless communication transceivers and pitot tubes are equipped in wind speed sensing payloads, which are lifted by aerostats.

The 3D wind profile is determined by the wind speed sensed by each sensing payload. The Pitot tube determines the wind speed relative to the payload. Positioned at the head and tail of the payload, the GPS receivers determine not only the direction of payloads but also the true position and velocity of the payload with respect to the ground. A wind profile is then calculated from the Pitot tube and dual GPS receivers.

Finally, the system is tested on a local wind farm. It has been shown that GPS provides a viable method for wind farm wind profile detection. The results of a field test conducted on a wind farm were shown to be consistent with averaged NOAA wind data during the time.

INTRODUCTION

Wind energy is currently one of the fastest growing sources of renewable energy. Wind turbines generate clean electricity without harmful emissions to the environment. However the volatile nature of wind and the resulting uncertainty in predicting wind power generation become a main barrier for wind energy penetration into the electricity grid. Traditional wind sensing is done through the construction of large meteorological masts with cup anemometers. Alternative wind sensing techniques entail alternative remote sensing methods to tower-based cup anemometers, such as light detection and ranging (LiDAR) and sound detection and ranging (SoDAR) [1, 2]. However these methods prove to be

costly, especially for offshore wind farms. Due to the complexity or size of terrain, wind farms often have uneven flow conditions. For example, the Roscoe Wind Farm in Texas covers 100,000 acres of land with 627 turbines. Taller, new generation wind turbines in the 10 MW class span as high as 200 meters at the blade tip, thus making structures such as traditional 60-meter anemometer masts even more unattainable. In addition, wake effects from neighboring turbines affect the wind flow of surrounding turbines causing a complex modeling of a farm's wind profile. Sensing the wind profile densely, accurately, in three dimensions, and inexpensively is critical for both optimizing the installation of wind turbines on a wind farm, and predicting and operating the power generation.

The cost of failing to achieve these can be severe for a wind farm operator. If low wind speeds aren't correctly predicted or monitored, a megawatt source of power could suddenly disappear and cripple an entire section of a power grid. Power must be diverted from other sources to compensate for the loss. There are also concerns for strong wind: wind turbines need to be shut off or tapered or the wind may cause damage to the turbines. In addition, generation of too much power may overload the grid and cause wind farm operators to be charged.

Existing cases of GPS based wind speed detection include the use of direct and reflected GPS signals collected off the surface of the ocean and analyzed for wind speed [3, 4, 5]. However this situation is not possible for wind farm use due to the high absorption of signals on the ground. In addition this technique is used to sense ocean surface winds whereas the concerns for wind turbine operators are at wind turbine altitude. Another case equips a UAV [6] with a Pitot tube and an inertial measurement unit to measure wind speed with a moving platform. This method is difficult to conduct on a wind farm because the multitude of moving objects may collide with a wind turbine. Without a tether line, this method can only be extended to short term monitoring and would not be able to map a constant wind profile.

This paper presents a novel system that allows for wide area 3D wind profile detection. The proposed approach uses a distributed array of GPS guided aerostats. Multiple aerostats are deployed with wind sensing payloads at different altitudes for 3D wind sensing.

The paper will first describe an overview of the system and how sensing will be accomplished. Afterwards it will detail the algorithms and methods used for wind speed sensing and creation of a wind profile. Finally, a prototype aerostat will be described and the results of a field test will be presented.

SYSTEM DESIGN

The proposed system is a tethered aerostat platform that flows freely in the air. The aerostat is composed of a lift system, a sensing system, and a ground station for data collection and post processing. The platform will be stationed near wind turbines with the sensing payloads level with the wind turbine blade centers. Figure 1 shows an example depiction of the system in operation.

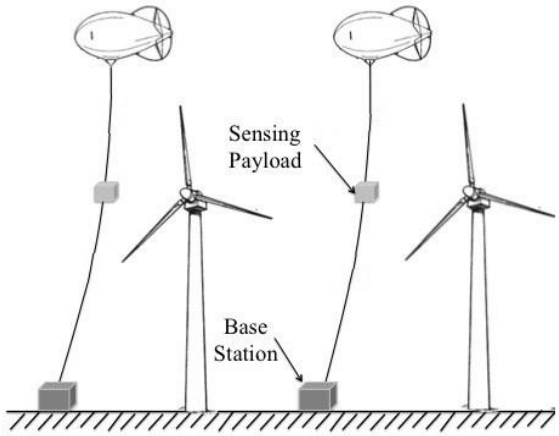

Figure 1. Concept depiction of wind sensing system in operation

This system is shown to be highly adaptable towards different wind farm parameters.

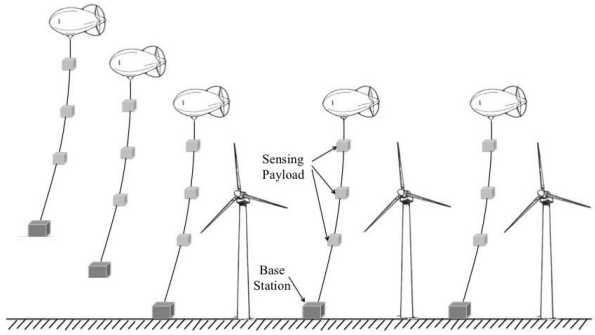

Figure 2: Summation of payload, relative and absolute wind velocities

Figure 2 shows the potential for scalability of the system. In order to obtain a higher resolution profile, multiple sensing payloads could be attached to a single tether line. Sensing of different altitudes and variations of wind turbine height can be accommodated for by altering the tether line length. In addition, larger wind farms can be covered by increasing the number of tethered aerostat platforms.

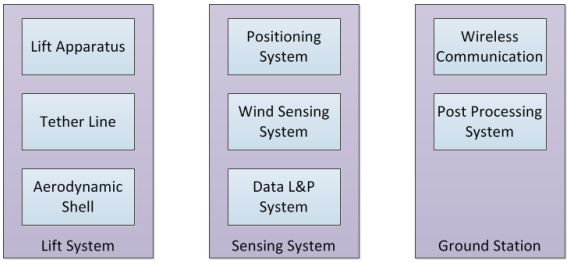

Figure 3. System Architecture of GPS-based Wind Sensing System

Figure 3 illustrates the different subsystem components that make up each of the larger functionality systems.

The lift system provides lift for the sensing payload, maintaining elevation of the sensors at wind turbine altitude for wind sensing. The tether line is used to keep control of the aerostat and maintain sensing around a particular area. The aerodynamic shell provides structure and housing for the sensing payload. In addition it provides the important task of maintaining attitude of the sensing payload facing into the wind. This prevents the need for actuation and control apparatus such as rotors or movable fins, reducing cost and simplifying operation of the system.

The sensing payload is composed of the positioning and wind sensing systems. The combination of data from these sensors allow for the determination of a true wind profile. Data is logged and transferred to the ground station for wind profile monitoring and post processing data analysis.

ALGORITHMS

The speed of an object moving through the air can be described of as:

$$\text{Absolute Windspeed} = \text{Absolute Payload Speed} + \text{Relative Windspeed} \qquad (1)$$

Using the relation between relative frames, the absolute wind speed can be determined from the addition of relative wind speed to the absolute ground speed of the payload wind sensor. Wind sensing has two important components, wind speed and wind direction. Due to the tethered dynamics of the aerostat and the hanging payload sensing package, simple derivation of the direction the payload is flowing is not enough to derive the heading of the wind. DGPS is used for derivation of the complete wind profile.

Wind speed relative to the moving sensor payload is determined through a differential pressure sensor, the Pitot tube. Eq. 2 provides the calculation of wind speed.

$$V_{airspeed} = \sqrt{\frac{2(\Delta P)}{\rho}} \qquad (2)$$

where ΔP is the differential pressure, ρ is the air density for airspeed calculation. A low-pass filter is used to eliminate variance and disturbances in the relative wind speed measurements from the sensitivity of the differential pressure sensor.

To obtain the payload speed and heading DGPS was used. The motion of the payload sensor is able to capture the dynamics of the sensor so that the absolute wind speed can be determined.

Implementation was accomplished with two GPS receivers installed on the payload package with the center of mass of the aerostat roughly equidistant between the antennae of the receivers.

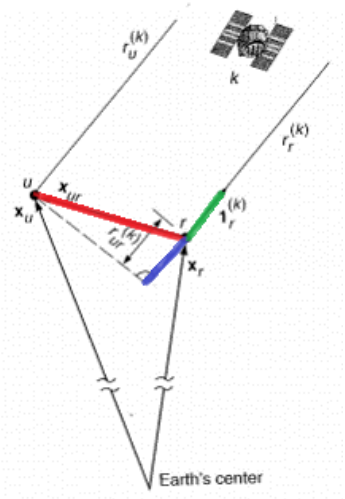

Figure 4: Overview of DGPS [6, 7]

Figure 4 shows an overview of differential GPS calculations. DGPS allows for the solution of the baseline vector, or the vector between the two receivers. The general DGPS equation is:

$$G(\vec{x}_u - \vec{x}_r) = (\vec{\rho}_u - \vec{\rho}_r) + \varepsilon \qquad (3)$$

where the projection of the baseline vector $\vec{x}_u - \vec{x}_r$ onto the satellite geometries matrix $G = [\mathbf{1}_r^{(1)} \quad \mathbf{1}_r^{(2)} \quad \cdots \quad \mathbf{1}_r^{(k)}]$ is equivalent to the matrix of range differences between the ranging of each GPS antenna to each satellite k in use plus additional errors **ε**.

Through the design aspect that the payload center of mass is halfway between the two antennae, the payload position is determined as $P_{payload} = P_r + \frac{\vec{x}_u - \vec{x}_r}{2}$. The derivatives of the payload position result in the magnitude of the wind velocity vectors.

A result of the design of the payload aerodynamic shell is that the sensor always restores to a trim position

facing into the wind. Relative wind positioning is always in the direction of the wind. The heading determination of the payload accounts for the remaining components of airspeed in the direction of the wind. The addition of the baseline vector gives the direction the sensor is pointing at, i.e. the direction opposite to the wind flow.

Because the antennae are in fixed locations across the payload sensor, a rigid baseline can be used to increase accuracy of attitude and positioning determination.

$$\min \left\| G\left(\vec{x}_u - \vec{x}_r\right) - \left(\vec{\rho}_u - \vec{\rho}_r\right) \right\| \quad (4)$$

The DGPS equation can be solved by minimizing the errors in the (4) such that the satisfying criterion $\vec{x}_u - \vec{x}_r = l$. However this constraint makes the optimization problem into a non-convex equation which is extremely difficult to solve. Because the calculated baseline vector from our data is shown to be greater than the length of the measured baseline, the constraint criterion can be changed to $\vec{x}_u - \vec{x}_r \leq l$. This allows the problem to be smoothly constrained and its convex properties restored for optimization.

HARDWARE IMPLEMENTATION

To test the effectiveness of the derived algorithms, the system was constructed and tested on a wind farm. The main objective of this experiment is to make a low-cost, accurate, and reusable system for 3D wind profile observation. Commercial off-the-shelf products were selected to reduce cost of the system. The system was designed with two subsystems, the Lift System and the Sensing System.

A. The Lift System

The Lift System consists of a helium balloon, a tether line, and an aerodynamic shell. It was designed to lift the wind sensing payload to the height of the wind turbine center at 50 meters. The helium balloon used to lift the payload is a 30ft diameter 1200g professional weather balloon. Tether line selected for the aerostat was a 100lb single fish line. The final component of the Lift System is the aerodynamic shell that houses the sensing and data processing payloads.

Design of the payload box optimized static stability to satisfy the pointing requirements of the sensor. Static margin (α) is a parameter used to quantify the static stability. It is defined by the equation

$$\alpha = d_{cp} - d_{cg} \quad (5)$$

where d_{cp} (d_{cg}) are the distance between the top of the nose cone to the center of pressure (gravity) of the payload box with devices. If $\alpha > 0$, the payload box has a positive margin, which means that when encounter a disturbance, a restoring moment to the equilibrium position will be generated. Thus, a payload box with positive margin will automatically align with the wind direction.

The amount of restoring moment is another important parameter when designing payload box. A payload box with excessive restoring moment will have excessive angular velocity when it reaches the equilibrium position and, as a result, deviate from the equilibrium position. Meanwhile, a payload box with insufficient restoring moment will return to the equilibrium position with a small angular velocity. Thus, both excessive and insufficient amount of restoring moment will longer the returning process of the payload box. The margin number (β) is used to character the amount of restoring moment with respect to the moment of inertia of the payload box. It is defined as

$$\beta = \frac{\alpha}{D} \quad (6)$$

where α is the static margin and D is the diameter of the base of the body tube. As a rule of thumb, a payload box with $1 < \beta < 2$ will have an ideal returning response to a disturbance.

The payload box is composed of a body tube, a nose cone, and three fins. The body tube is 22.5" in length and 5.54" in diameter. The nose cone is 13" in length and is attached to one end of the body tube. Three 4.00" spin fins are attached 1.50" away from the other end. The total mass of the payload box was weighed at 30.55 oz. The devices inside the box are simulated as a 70.55 oz point mass positioned 8.00" away from the tip of the nose cone. Thus, the total mass of a data collecting unit is 101.1 oz.

Assuming the density of every point of each component is a constant, each component can be modeled as a point mass located on its geometric center. The payload system is simulated as four point masses and the combined center of mass calculated as:

$$d_{cg} = \frac{m_{body}d_{body} + m_{nose}d_{nose} + m_{fins}d_{fins} + m_{devices}d_{devices}}{m_{Total}}$$

where m is the mass of the component, and d is the distance between the tip of the nose cone and the geometric center of the component.

Unlike the center of gravity, it is difficult to accurately calculate the position of the center of pressure without experiment. Normal forces acting on each component is highly dependent on the geometric shape, which is described by parameters found only through wind tunnel experiment. Instead of directly calculating the center of pressure, RockSim® was used to simulate the center of pressure.

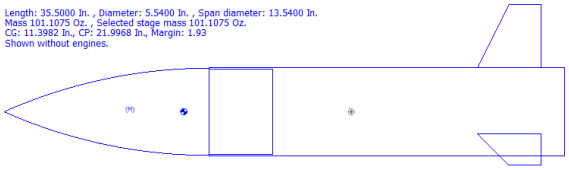

Figure 5: Aerodynamic Shell Design and RockSim simulation results

Figure 5 shows the results of the simulation where the center of gravity of the payload is 11.4" from the tip while the center of pressure is 22.0" from the tip. The resulting margin number is calculated as 1.93, which satisfies the foremost criterion of static stability.

Besides attitude, lift was also a necessary design criterion for the system. A weather balloon filled with helium was tasked with lifting the aerostat to sensing range. Design of the balloon size and helium amount was necessary to ensure that the system could be lifted by the balloon.

$$F_{buoyant} = \rho_{air} g V_{balloon} \quad (7)$$

$$F_{buoyant} > mg \quad (8)$$

Equations 7 and 8 showed the design criterion of the lift apparatus. The lift of helium balloons results from buoyant force and correlates directly to their volumes. The balloon was chosen so that the buoyant force was larger than the weight of the balloon and payload such that the balloon would rise and stay airborne while tethered. The desired altitude of the system can be controlled through adjustment of the tether line.

B. The Sensing System

The sensing system consists of 3 components, the wind sensing system, the positioning system, and the data logging and processing system. As shown in Figure 6, most of the electrical hardware is housed in the nose cone of the aerodynamic shell. The center of mass of the system is along the tether point.

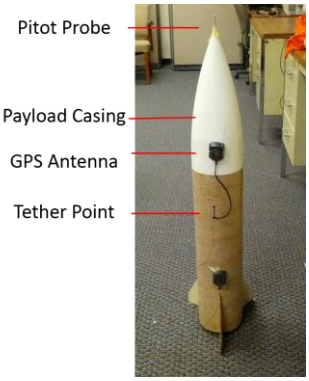

Figure 6: Payload Sensing System

The wind payload system consists of a Freescale Semiconductor differential air speed sensor or pitot probe, and an Arduino Uno microcontroller. The Arduino Uno is used to relay power to the airspeed sensor and translates the analog voltage differences into a digital reading for collection. The Pitot probe is placed protruding the nose cone of the payload shell, pointed towards the wind. The sensor collects differential pressure measurements that translate to relative wind speed measurements during post-processing.

The positioning system consists of two u-blox LEA-6T receivers and two u-blox ANN-MS-0-005 GPS antennae. The receivers were selected to be a low-cost, commercially available receiver that could be used to obtain raw data such as pseudorange, carrier phase, and Doppler shift.

The data logging and processing system consists of a Raspberry Pi, a USB hub, and a Powergen portable USB power supply. The Raspberry Pi includes the ability to log data on the operating SD card and host an Edimax Wifi adapter. Most of the on-board real-time processing is used to collect data and parse out data packets into an post-processable format. The data was streamed in real-time to a ground processing system while the WiFi link was in place. However since the sensing altitude is out of communications range, the complete set of data was extracted from the SD card after landing.

Figure 7: shows the assembled system in preparation for deployment and sensing.

The aim of this test was to create an inexpensive and accurate method of wind profile determination. This was accomplished with the use of precise GPS positioning paired with relative wind speed sensing for wind speed determination. While other systems may cost over tens of thousands of dollars, for our system, the cost of a single aerostat platform and sensor, as shown in Table 1, came to under $700 USD.

Table 1.Wind Sensing System Component Costs

Component	Cost (USD)
GPS Receivers and Antennae (2)	$300
Wind Sensing System	$50
Data Logging and Processing System	$60
Helium Balloon	$100
Helium	$120
Aerodynamic Structure	$45
Total	$675

FIELD TEST AND RESULTS

An experimental field test was conducted on June 3rd, 2013 at a local wind farm in Paxton, IL. The system was set up to verify its effectiveness of the system for wind profile determination.

Figure 8: System in operation as well as a few wind turbines in the background.

Results of the test showed that although the u-blox LEA-6T provides consistent data on the ground, due to the highly erratic dynamics of the aerostat, the u-blox receivers lose their tracking loops while in the air. As a result multiple cycle slips and data gaps occur in the resultant GPS data. It was found that after leaving the more stable flow of air near the ground, the longest continuous segment of errorless data was 29 seconds and multiple segments were divided by gaps of an average of 8 seconds each.

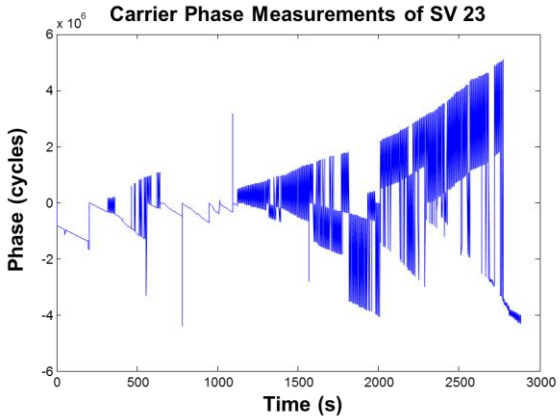

Figure 9: Multiple cycle slips occurred due to the erratic dynamics of the aerostat.

Figure 9 shows carrier data collected from the field test of SVN 23. The data consisted of multiple gaps and had to be cleaned before processing. In order to obtain the wind profile of the entire period of time, filtering was incorporated for estimation of the payload sensor attitude and velocity when GPS data was unavailable.

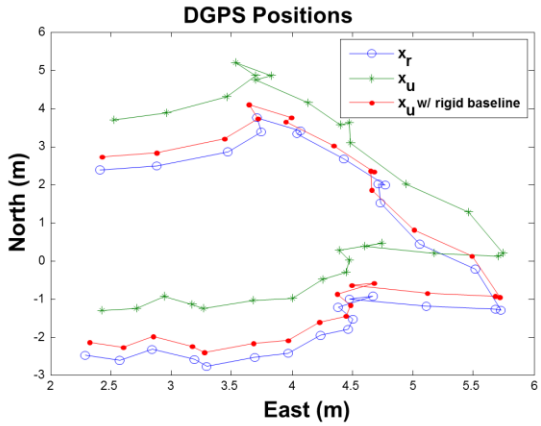

Figure 10: DGPS Positions of the user and reference receiver antennae on-board the sensing payload.

Figure 10 shows the path of the aerostat over the measurement period. Carrier smoothed data was used to obtain initial receiver positions for reference calculations. Afterwards DGPS was applied to obtain the locations of the user or foremost receiver. The constraint of applying the rigid baseline allowed for a much more accurate solution of the position and attitude of the baseline. By constraining the baseline to the measure length of .35m, the calculated baselines across the period of data remained consistent.

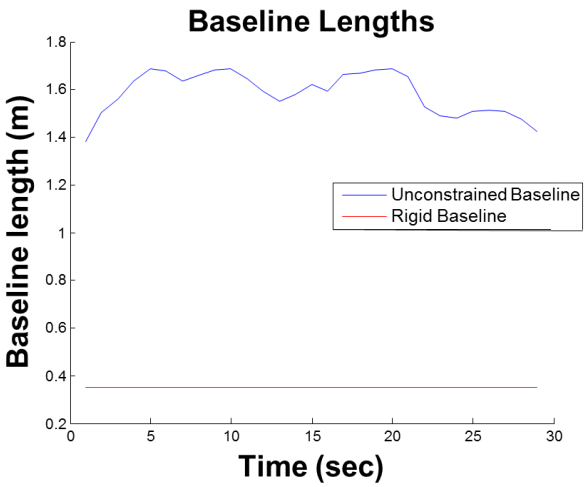

Figure 11: DGPS Positions of the user and reference receiver antennae on-board the sensing payload.

Figure 11 shows the results of the baseline constraints. Because calculated baselines during the period of data collection were greater than the rigid measurement of .35, the optimization parameters could be altered due to the smooth nature of the optimization problem. Solution of the non-convex problem is currently being worked on as future work.

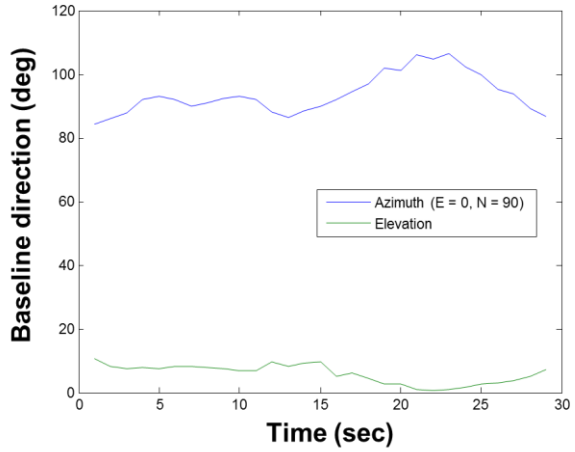

Figure 12: Baseline direction for sensing payload attitude determination

From the result of the baseline, the attitude and pointing of the system could be determined. Figure 12 shows that the sensing payload remained relatively flat and pointed northwards towards the period of data analysis presented. Next the addition of payload sensor velocities and relative wind velocities yielded wind velocity.

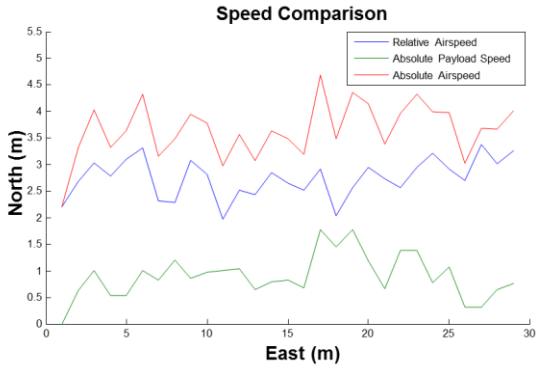

Figure 13: Summation of payload, relative and absolute wind velocities

Figure 13 shows that the addition of the 3D velocities of each component for wind profile determination. The selected period of data to analyze was chosen when the aerostat was close to the ground. This is because we were unable to obtain field anemometer data and thus NOAA's surface wind data was used as ground truth. During the period of time, NOAA recorded an average of 4.1 m/s of wind data. This data is shown to correlate with our wind speed results. It is important to note that wind speeds are lower while close to the ground due to the results of drag. As elevation increases to the range of 50m, wind is shown to reach upwards of 12 m/s.

Taking the result of the wind speed magnitudes and the attitude, a quiver plot was constructed above the center of mass positions of the system.

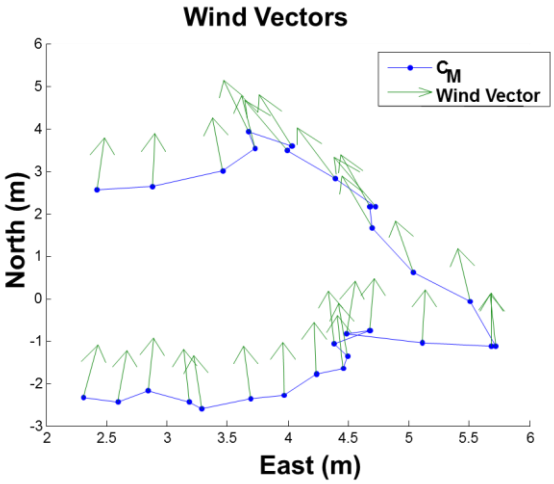

Figure 14: Quiver plot of wind velocities and heading on the payload center of mass

Figure 14 shows the wind vectors plotted on the center of mass, or the tether point of the aerostat. It is important to note that the aerostat does not travel in the direction of the wind due to tethering of the aerostat. However it is assumed that the magnitude of velocity of

the aerostat is entirely captured within relative wind measurements and the magnitude of position changes with tethering.

DGPS was also proven to be effective in determining wind heading. As the elevation with the rigid baseline in place remained fairly constant, the payload package was determined to be quite level. The azimuth determined the direction of the heading of the aerostat and was shown to be pointed north.

CONCLUSION

This paper presented a novel 3D wind profile sensing method based on precise aerostat positioning and differential pressure-based relative airspeed measurements. A cost-efficient prototype was constructed to test the proposed algorithms and system operation on a wind farm. GPS is was proven to provide a viable and inexpensive method for wind farm wind profile detection. The results of a field test conducted on a wind farm were shown to correlate with averaged NOAA wind data during the time.

FUTURE WORK

Future work involves extending the endurance of the aerostat platform for longer wind farm monitoring. Currently monitoring capabilities are limited by the battery length powering the system to a length of around 3 hours. For a permanent fixture, the tether line can be used as a supply line for power and helium for continual lift. In addition, data may be sent through the line for real time monitoring or an additional wireless communication adapter may be installed into the system.

It is shown that although low-costs components provide a reasonable reading of the wind profile, the use of higher quality sensors may increase the accuracy of the determined profile. Higher quality, but still low costs GPS receivers may be able to reduce the errors from the cycle slips and loss of tracking loops. Better onboard differential relative pressure sensors will be able to provide a more accurate and finer relative wind sensing resolution.

ACKNOWLEDGEMENTS

The authors would like to thank the following for their help in allowing this project to be a success:

Larry and Sue Ballinger for letting us conduct our field tests in their wind farm in Paxton, IL.

Lori Ballinger-Pankau for helping us connect with the wind farm owners and set up a field test.

Oliver Cai, with his knowledge of flying model aircraft, for his assistance in the field test.

REFERENCES

[1] Hasanger C, Peña A, Christiansen M, Astrup P, Nielsen M, Monaldo F, Thompson D, Nielsen P., “Remote sensing observation used in offshore wind energy,” *IEEE Journal of Selected Topics in Applied Earth Observations and Remote Sensing*, 2008 1(1): 67-79.

[2] Bingöl, Ferhat, Jakob Mann, and Gunner C. Larsen. "Light detection and ranging measurements of wake dynamics. Part I: one-dimensional scanning." *Wind Energy* 13.1 (2010): 51-61.

[3] Yu, Kegen, Chris Rizos, and Andrew Dempster. "Sea surface wind speed estimation based on GNSS signal measurements." *2012 IEEE International Geoscience and Remote Sensing Symposium (IGARSS)*, 2012.

[4] Komjathy, A., Armatys, M., Masters, D., Axelrad, P., Zavorotny, V.U., Katzberg, S.J., "Developments in Using GPS for Oceanographic Remote Sensing: Retrieval of Ocean Surface Wind Speed and Wind Direction," Proceedings of the 2001 National Technical Meeting of The Institute of Navigation, Long Beach, CA, January 2001, pp. 753-761.

[5] Armatys, M., Masters, D., Komjathy, A., Axelrad, P., Garrison, J. L., "Exploiting GPS as a New Oceanographic Remote Sensing Tool,"Proceedings of the 2000 National Technical Meeting of The Institute of Navigation, Anaheim, CA, January 2000, pp. 339-347.

[6] Cho, A., Kim, J., Lee, S., and Kee, C., "Wind Estimation and Airspeed Calibration using a UAV with a Single-Antenna GPS Receiver and Pitot Tube". IEEE Transactions on Aerospace and Electronic Systems. v47. 109-117.

[7] Cohen, C. E., “Attitude determination using GPS,” PhD thesis, Stanford University, 1992.

[8] Pratap M., and Enge, P., “Global Positioning System: Signals, Measurements, and Performance, (Revised Second Edition)”, Ganga-Jamuna Press, Dec, 2010.